JCTC Journal of Chemical Theory and Computation

Single Stranded Loops of Quadruplex DNA As Key Benchmark for Testing Nucleic Acids Force Fields

Eva Fadrná,[†] Nad'a Špačková,[‡] Joanna Sarzyñska,[§] Jaroslav Koča,[†] Modesto Orozco,[∥] Thomas E. Cheatham III,[⊥] Tadeusz Kulinski,[§] and Jiří Šponer*,[‡]

National Centre for Biomolecular Research, Faculty of Science, Masaryk University, Kotlářská 2, 611 37 Brno, Czech Republic, Institute of Biophysics, Academy of Sciences of the Czech Republic, Královopolská 135, 612 65 Brno, Czech Republic, Institute of Bioorganic Chemistry, Polish Academy of Sciences, Noskowskiego 12/14, 61 704 Poznań, Poland, Joint IRB-BSC program on Computational Biology, Institute for Research in Biomedicine, Baldiri Reixac 10-12, 08028 Barcelona, Spain, Barcelona Supercomputing Center, Jordi Girona 29, 08034 Barcelona, Spain, Department of Biochemistry, University of Barcelona, Diagonal 647, 08028 Barcelona, Spain, and Departments of Medicinal Chemistry and of Pharmaceutics and Pharmaceutical Chemistry, University of Utah, 30 South 2000 East, Salt Lake City, Utah 84112

Received April 24, 2009

Abstract: We have carried out a set of explicit solvent molecular dynamics (MD) simulations on two DNA quadruplex (G-DNA) molecules, namely the antiparallel $d(G_4T_4G_4)_2$ dimeric quadruplex with diagonal loops and the parallel-stranded human telomeric monomolecular quadruplex d[AGGG(TTAGGG)$_3$] with three propeller loops. The main purpose of the paper was testing of the capability of the MD simulation technique to describe single-stranded topologies of G-DNA loops, which represent a very challenging task for computational methods. The total amount of conventional and locally enhanced sampling (LES) simulations analyzed in this study exceeds 1.5 μs, while we tested several versions of the AMBER force field (parm99, parmbsc0, and a version with modified glycosidic χ torsion profile) and the CHARMM27 force field. Further, we compared minimal salt and excess salt simulations. Postprocessing MM-PBSA (Molecular Mechanics, Poisson−Boltzmann, Surface Area) free energy calculations are also reported. None of the presently available force fields is accurate enough in describing the G-DNA loops. The imbalance is best seen for the propeller loops, as their experimental structure is lost within a few ns of standard simulations with all force fields. Among them, parmbsc0 provides results that are clearly closest to the experimental target values but still not in full agreement. This confirms that the improvement of the γ torsional profile penalizing the γ trans substates in the parmbsc0 parametrization was a step in the right direction, albeit not sufficient to treat all imbalances. The modified χ parametrization appears to rigidify the studied systems but does not change the ultimate outcome of the present simulations. The structures obtained in simulations with the modified χ profile are predetermined by its combination with either parm99 or parmbsc0. Experimental geometries of diagonal loops of $d(G_4T_4G_4)_2$ are stable in standard simulations on the ~10 ns time scale but are becoming progressively lost in longer and LES simulations. In addition, the $d(G_4T_4G_4)_2$ quadruplex contains, besides the three genuine binding sites for cations in the channel of its stem, also an ion binding site at each stem-loop junction. This arrangement of five cations in the quadruplex core region is entirely unstable in all 24 simulations that we attempted. Overall, our results confirm that G-DNA loops represent one of the most difficult targets for molecular modeling approaches and should be considered as reference structures in any future studies aiming to develop or tune nucleic acids force fields.

10.1021/ct900200k CCC: $40.75
Published on Web 08/19/2009

Introduction

Guanine rich sequences are known to occur in many positions of the genome and are especially common at the chromosome ends, the telomers. Such sequences readily form four stranded guanine quadruplex structures (G-DNA) *in vitro*, and it is believed that the same could happen with telomeric sequences (such as the human one: $d(TTAGGG)_n$),[1] where repetitive double stranded segments are followed by single strand overhangs of the same repeat. Such overhangs can fold back defining a quadruplex, whose formation could protect them from being accessed by reverse transcriptase enzyme telomerase. Telomerase is active in most cancer lines and contributes to their immortality by maintaining the length of the overhang.[2] Thus, it has been suggested that compounds stabilizing G-DNA *in vivo* can act as anticancer drugs.[3,4] There are also other biological or pharmacological roles that have been suggested for G-DNA[5] which together with the increasing number of applications of the quartet structures in nanosciences[6,7] makes G-DNA the most important noncanonical DNA architecture, explaining the very intense research focused in the last years in this molecule.[8−13]

The basic structural element of G-DNA is a quartet involving four cyclically bonded guanines that are interconnected by hydrogen bonds (Figure 1a). The quartets are further stabilized by monovalent ions placed along the central channel of the structure and interacting with O6 atoms of the guanines, compensating the highly electronegative electrostatic potential region in the quartet centers (Figure 1a). Several (usually 2−4) consecutive quartets form a G-DNA stem and the cations fill its channel, being either in planes of the quartets or in the cavities between them. The stem can be created by 1, 2, or 4 separate DNA pieces and thus there are intramolecular (unimolecular), dimeric (bimolecular), or tetramolecular quadruplexes. The adjacent strands of the G-DNA stem may run either in parallel or antiparallel fashion. The guanines are in anti orientation in the all-parallel stems while antiparallel arrangements have to utilize also some syn nucleotides. The stems of bimolecular and intramolecular quadruplexes are supplemented by single stranded (mostly thymine-rich) loops which are formed by the nucleotides interdispersed between the guanine stretches forming the stem strands. The loops can be placed above the planes of the terminal quartets of the stem, and then they can link either adjacent or diagonal guanines, resulting into lateral or diagonal (Figure 1b) loop arrangements. Alternatively, the loops can run across the G-DNA grooves, from top to bottom (or bottom to top) of the quadruplex stem. These are called propeller, groove, or chain-reversal loops (Figure 1c).

G-DNA molecules have been extensively studied by atomic resolution experiments and other experimental approaches that have provided unique insights into many aspects of G-DNA structural, dynamical, and kinetic properties.[5,16−31] One of the amazing features of G-DNA with loops is their enormous structural polymorphism, where a given sequence can adopt multiple folds and often subtle changes in the sequence or environment (such as type of ions) may have large effect on the topology.[19,20,32−39] This G-DNA structural variability may be reminiscent of the complexity of rules governing topologies of nucleic acids junctions.[40]

Theoretical methods have been also widely applied to investigate various aspects of G-DNA,[41−69] for a recent review see ref 65. Among the different theoretical methods for the study of G-DNA atomistic molecular dynamics (MD) with explicit solvent is probably that able to capture with higher accuracy the structure and dynamics of G-DNA in aqueous solution. Unfortunately, when using MD simulations we cannot ignore that they are based on simple empirical force fields which can lead to artifacts in simulations. This means that testing and benchmarking become a crucial step to validate the reliability of any simulation. Earlier studies indicated a very good performance of the simulation technique in studies of G-DNA stems, except for some modest imbalance of the cation positions within the stem.[62] It was observed that the ions look oversized (too large) and avoid in-plane positions in the quartets even when simulated with Na^+. Bifurcated bonding of the quartets was also often noticed, which is a perturbation of the structure compared to the experiments. These problems were tentatively attributed to the lack of polarization term in the pair additive classical force field, which was also confirmed by quantum - chemical calculations showing that the strength of direct cation - G(O6) interactions is underestimated with a too early onset of short-range repulsion. Besides that, the simulations revealed that the cation-stabilized stem is a uniquely rigid molecular assembly and the ions are necessary for its stabilization.[62,66] However, the quadruplex stem is still stable with a reduced number of ions in the channel, which allows a smooth exchange of ions with the bulk solvent. An initially empty stem is capable to attract a bulk ion swiftly,[63] thus, in reality, G-DNA stems should never be left vacant by cations. Alternative topologies of G-DNA stems were found, with shifted (slipped) strands.[62,70] The possibility of such substates was later confirmed by experiments.[71] Further studies demonstrated that guanine to thioguanine substitution significantly sterically destabilizes the stem while inosine causes only its subtle destabilization.[64,66] However, inosine may interfere with the process of G-DNA stem formation, by destabilization of kinetic intermediates that rely on interbase H-bonding, before the ion binding starts to dominate the stabilization.[66,70] Simulations were also used to investigate a wide range of double, triple, and quadruple stranded species that could occur as intermediates during quadruplex stem formation[70] and to analyze the properties of G-DNA under hostile conditions such as vacuum, something relevant to rationalize mass field spectroscopy experiments.[21,61,72]

Our subsequent attempt to in-depth characterize the loop topology of the *Oxytricha nova* $d(GGGGTTTTGGGG)_2$ (or

* Corresponding author phone: +420 5415 17133; fax: +420 5412 12179; e-mail: sponer@ncbr.chemi.muni.cz.
† Masaryk University.
‡ Academy of Sciences of the Czech Republic.
§ Polish Academy of Sciences.
|| Institute for Research in Biomedicine, Barcelona Supercomputing Center, and University of Barcelona.
⊥ University of Utah.

$d(G_4T_4G_4)_2$) quadruplex using simulations indicated inadequacy of the major nucleic acids molecular modeling force field AMBER (versions parm94 - parm99)[73−75] for this particular task.[45] In standard simulations, the diagonal loops were basically stable as taken from the starting experimental structures. However, the ions residing at the stem-loop junction in the X-ray structures were lost. In contrast, locally enhanced sampling (LES)[76,77] molecular dynamics simulations aimed at finding the global loop minimum independently of the starting structure predicted entirely different loop geometry, which was in clear disagreement with the experimental structures. Note that the experimental geometry of the $d(G_4T_4G_4)_2$ loop has been unambiguously determined by independent X-ray and NMR studies which are mutually entirely consistent.[14,30,78] Subsequent free energy computations indicated that the predicted incorrect loop topology is more stable according to the force field than the correct experimental one, further suggesting that the force field is in trouble and that we were not facing a LES-artifact. These negative results pointed out the difficulties in representing loops by current force fields, which have been always parametrized considering canonical helices or highly compact RNA structures. These results suggest loops as an excellent benchmark to test the accuracy of current force fields to describe highly irregular nucleic acid structures.

In the present paper we substantially expand the G-DNA loop calculations, using them as a benchmark of the quality of current force fields to describe unusual DNA structures. Besides the $d(G_4T_4G_4)_2$ dimeric quadruplex with diagonal loops we study also the parallel stranded human telomeric monomolecular quadruplex $d[AGGG(TTAGGG)_3]$ with three propeller loops, as revealed by X-ray crystallography.[15] The present study was motivated by recent refinements in well established force fields, some of them which provide a dramatic improvement in simulations of canonical nucleic acid structures and that were robust in the microsecond time scale.[79] Particularly, we tested the older version of amber force field for nucleic acids, parm99[74] and its parmbsc0 refinement.[79] Further, we employed another version of AMBER force field,[80] which changed the glycosidic torsion profile and which can be combined with either parm99 or parmbsc0 AMBER force fields, and the latest version of the CHARMm force field,[81,82] which is known to produce reasonable trajectories for canonical DNAs (for a recent comparison with parmbsc0 see ref 83), but that has not been much used to study noncanonical DNA structures. Further, we considered also diverse cation parameters to check the importance of counterions parametrization in the calculations. Explicit solvent molecular dynamics simulations are complemented by locally enhanced sampling simulations and postprocessing MM-PBSA (Molecular Mechanics, Poisson−Boltzmann, Surface Area) free energy calculations.[84,85]

Our results reveal that none of the presently available force fields is accurate enough in describing the G-DNA loops. The imbalance is best seen for the propeller loops, as their experimental structures are lost even during standard simulations. Among the force fields, parmbsc0 provides results that are closest to the experimental target values but still not in full agreement. This indicates that the improvement of the γ torsional profile penalizing the γ trans substate was a step in the right direction, albeit not sufficient to treat all imbalances. The modified χ parametrization appears to rigidify the studied systems but does not change the ultimate outcome of the simulations. The structures obtained in simulations with the modified χ profile are predetermined by its combination with either parm99 or parmbsc0. Overall, our results confirm that loops in guanine quadruplex molecules represent a very difficult target for molecular modeling approaches and should be considered as references in any future studies aiming to develop or tune nucleic acids force fields. Properly tuned force fields, designed to reproduce these complex motifs can provide improved description of many other types of nucleic acids. Note nevertheless that the existing variants of the AMBER force field were shown to be successful in the description of a wide range of noncanonical structures, including many complex RNAs,[86,87] and also the G-DNA and i-DNA stems,[65] underlining the unique complexity of the loop simulations.

Methods

Starting Geometry and Initial Model Building. The initial structures were taken from the following experimental structures: the X-ray structure of the $d(G_4T_4G_4)_2$ sequence from the 3′ overhang of the *Oxytricha nova* telomere (NDB: UD0014, PDB: 1JRN, resolution 2.00 Å)[14] and the X-ray structure of the human telomeric quadruplex sequence $d[AGGG(TTAGGG)_3]$ (NDB: UD0017, PDB: 1KF1, resolution 2.10 Å)[15] (Figure 1b,c).

The earlier simulations of the $d(G_4T_4G_4)_2$ quadruplex which are also assessed in this paper were based on the NMR structure (PDB: 156D).[30,88] The NMR structure is, when utilized as starting structure for MD simulations, basically equivalent to the X-ray structure (there are modest structural differences within the same substate of the loop geometry) except for the absence of monovalent ions at the stem-loop junction (see below). The NMR experiment could not capture positions of the ions. Some test simulations of parallel tetramolecular quadruplex $d(G_4)_4$ started from the X-ray structure (PDB: 352D)[26] or the human telomere structure (for $d(G_3)_4$) where propeller loops were deleted.

All simulations started with the structural monovalent ions fully occupying the G-DNA stem (three and two ions for the Oxytricha (OXY) and human telomeric (HT) G-DNA, respectively). In most simulations of $d(G_4T_4G_4)_2$, structural ions were initially also placed at the stem-loop junction based on their experimental positions (initially 5 ions in the structure, see Figure 1b). Also the HT G-DNA X-ray structure shows a monovalent ion above the upper quartet plane that was included in some starting structures. This ion, however, evidently is not an integral part of the quadruplex, since it is sandwiched between two adjacent stems in the crystal structure. This ion is never stable in simulations.

Note that the HT quadruplex sequence is known to adopt variable topologies with different types of loops depending on the experimental conditions.[89−91] However, analysis of the topological variability of this sequence is outside the scope of this study. The X-ray structures are the most suitable

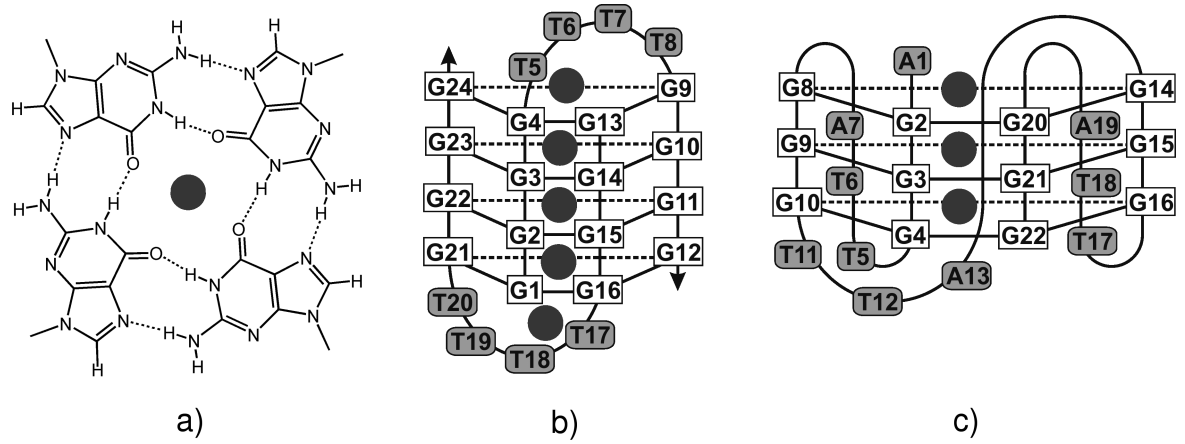

Figure 1. Scheme of a) the guanine quartet and the studied experimental structures of b) the bimolecular antiparallel quadruplex formed by the *Oxytricha nova* telomeric sequence[14] $d(G_4T_4G_4)_2$ with four quartets, two close-to-identical diagonal loops, three stem K^+ ions, and two K^+ stem-junction ions and c) unimolecular parallel quadruplex with three very similar propeller (groove, chain-reversal) loops formed by the human telomeric sequence[15] d[AGGG(TTAGGG)$_3$] with K^+ stem ions. The ion above the upper quartet is a result of crystal packing.

ones for comparison with simulations aimed at force field testing. Since the simulations were unable to keep correct experimental loop structures for the above two G-DNAs, it was not necessary to extend the simulations to other systems.

AMBER Simulations. The structures were prepared by the xleap module of AMBER (adding of hydrogen atoms and neutralizing the system by adding monovalent counterions, either K^+ or Na^+, with numerous control KCl excess salt simulations). The net-neutralizing ion condition leads to a cation concentration of ~0.3 M and ~0.2 M for OXY and HT systems, respectively (the OXY system is more compact and thus the box has less water molecules per nucleotide). When using excess salt we set the cation/anion ratio to be 2:1, resulting in ~0.5 M cation concentration (~0.2 M and ~0.3 M excess salt) for the OXY and HT systems. The solute was embedded in TIP3P water box,[92] which was extended approximately 10 Å in each direction from the solute. Some simulations were done also with the SPC/E water model.[93] Different ion parameters were tested, as specified below. There were ~13000 and ~18000 atoms in OXY G-DNA and HT G-DNA simulations, respectively.

AMBER Force Fields. The AMBER simulations were carried out with the parm99,[74] parmbsc0,[79] and Ode et al.[80] versions of the Cornell et al. force field.[73] Parm94 version[73] was not tested, but its performance is expected to be very similar to the parm99. In contrast, parmbsc0 introduces a substantial modification of the α/γ torsional backbone parameters which is absolutely essential to stabilize B-DNA simulations. Parmbsc0 has been verified extensively by simulations. The Ode et al. force field suggests reparametrization of χ glycosidic torsion and can be combined either with parm94−99 or parmbsc0. The Ode et al. force field has not been tested in simulations so far, except for a few 5 ns runs[80] which we consider as entirely insufficient testing.

Cation Parameters. The pair additive nonpolarizable force field approximation limits the quality of description of the cation - solute interactions. Nevertheless, we tried different cation parametrizations to see if they can affect the results.

We mostly used standard AMBER potassium (radius 2.6580 Å and well depth 0.000328 kcal/mol) and sodium (radius 1.8680 Å and well depth 0.00277 kcal/mol) parameters. We also used K^+ ions with smaller radii (K^+ reduced, radius 2.4 Å and well depth 0.0011 kcal/mol or 2.5 Å and well depth 0.0008 kcal/mol). The reason for the reduction of the ion radii is the observation that the original K^+ ions appear to be oversized (having too large radius) in the G-DNA ion channel, leading sometimes even to expulsions of K^+ out of the channel (see below).

The extent of deficiency of the force field description of the solute - ion interactions is nicely visualized by comparing quantum chemical evaluation of the O6(G)...K^+ interaction energy with force field calculations (Figure 2). The force field underestimates the interaction energy and overestimates the repulsion for shorter O6...K^+ distances. Our parameter adjustment for K^+ (K^+ reduced) was qualitatively based on the quantum-chemical calculations and should be considered as specific for G-DNA simulations. We do not claim that these parameters are better than the original ones for common simulations. It is not possible to simultaneously fully balance all solute - ion and solvent - ion interactions with such simple pair-additive force fields. Obviously our ion parameter adjustment reduces the O6...K^+ repulsion but does not lead to a full agreement since the binding energy remains sharply underestimated due to lack of polarization in the force field. Besides the neglect of polarization, the 6−12 Lennard-Jones force field term is likely excessively repulsive (too steep) in the short-range region.

There have been recent systematic efforts to refine the monovalent ion parameters for AMBER nucleic acids simulations.[94] These efforts, however, were directed to improve the bulk behavior of the ions. As shown in Figure 2, all presently available cation force fields provide essentially similar interaction energy curves with the guanine O6, which exaggerates the short-range repulsion and underestimates the attraction. That is a natural consequence of the pair additive force field which offers just two parameters to be adjusted, the radius and well depth. It is not possible to

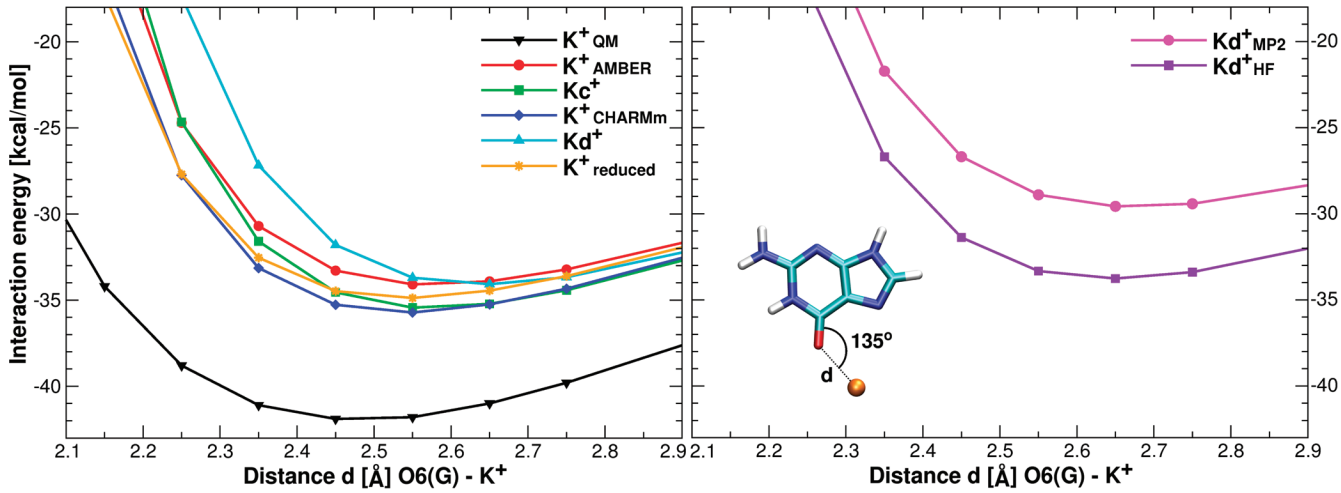

Figure 2. Left - the dependence of the interaction energy between G(O6) and K^+ in a G-DNA like geometry. Black (triangle down), reference QM data with inclusion of electron correlation, Becke3LYP/6-311G(d,p) method corrected for basis set superposition error; red (circle), standard AMBER parameters (2.6580 Å, 0.000328 kcal/mol); blue (diamond), standard CHARMm parameters (1.76375 Å, 0.087 kcal/mol); orange (star), parameters for ions with reduced atomic radii (2.4 Å, 0.0011 kcal/mol); green (square), parameters Kc^+ by Joung and Cheatham[94] (1.7050 Å, 0.1936829 kcal/mol); and cyan (triangle up) parameters Kd^+ by Dang[95] (1.8700 Å, 0.100 kcal/mol). Data in parentheses represent atomic radii and potential well depths. All force fields underestimate the stabilization and exaggerate the short-range repulsion (the optimal O6...K^+ distance and namely the gradient of the energy in the repulsive region). Note that despite the variability of parameters all the force fields cluster in a narrow region rather far from the QM data, indicating that the simple force field function is not sufficient to reproduce the QM data. Specifically, once the ion force fields are tuned to reproduce target condensed phase bulk solvent and ion−ion data, there are no more free parameters to optimize the cation - solute interactions. Comparison for Na^+ would result in a similar picture. Right - comparison of force field calculation with HF (AMBER) ESP charges and ESP charges derived with the inclusion of electron correlation (MP2/aug-cc-pVDZ level, the upper curve).

simultaneously satisfy the ion hydration reference data (or other bulk properties) and direct solute - cation interactions. Interestingly (Figure 2 right), when the force field is combined with MP2 charges instead of the HF ones, the gap between the reference QM data and the force field curve further widens, despite the fact that the MP2 charges should at first sight bring the QM and force field closer to each other (because both computational methods then have electrostatic terms reflecting electron correlation effects). The fact that the HF charge distribution brings the force field calculations closer to the full QM curve than the charge distribution derived with electron correlation is due to partial compensation of errors. The HF charges exaggerate the polarity of the electrostatic potential, and thus the electrostatic attraction between the cation and the guanine is overestimated, partially counterbalancing the missing polarization effects.

In our simulations, we also tested potassium parameters published by Dang[95] (atomic radius 1.8700 Å and well depth 0.100 kcal/mol) and parameters by Joung and Cheatham[94] (atomic radius 1.7050 Å and well depth 0.1936829 kcal/mol). We also carried out some simulations in higher salt conditions using KCl. In these simulations, both potassium and chloride ions were described by Dang parameters which in the case of chloride (radius 2.47 Å, well depth 0.1 kcal/mol) represent standard AMBER parameters.

Standard AMBER Molecular Dynamics Simulations. Molecular dynamics simulations were performed with the Sander module of the AMBER-5.0−9.0 software package.[96−100] The particle mesh Ewald (PME) method[101] was used for a correct treatment of electrostatic interactions. All simulations were run with the SHAKE algorithm[102] (with a tolerance of 0.0005 Å) to constrain covalent bonds involving hydrogens, with periodic boundary conditions, a 2-fs time step, and a temperature of 300 K (Berendsen temperature coupling algorithm with time constant of 0.2 ps[103]). Standard equilibration and production procedures were applied. Analyses of resulting trajectories were performed with ptraj or carnal modules, and the results were visualized with the help of VMD graphic software[104] and X3DNA.[105] The protocol is described in more detail in our recent studies.[106,107]

Locally Enhanced Sampling Molecular Dynamics Simulations (LES). The locally enhanced sampling (LES) method[76,77] was performed with an addles module of AMBER to divide the structure into regions (stem and loops), and each of the loops was split into 5 independent copies. Force field parameters for the copies were adjusted accordingly which lowers the energy barriers. In order to provide an initial "kick" to the 5 copies, the structure was heated to 500 K. Moreover a long relaxation phase appears vital to provide sufficient freedom for the copies to settle in different regions of the conformational space. To allow for this, the temperature was gradually decreased from 500 to 300 K over 1.5 ns (during the first 750 ps the pressure was set to 100 atm), and guanine quartets were maintained with flatwell restraints (R1 = 0.0, R4 = 6.0, RK2 = 5.0, RK3 = 10.0; R2 and R3 depend on the actual distance R between the restrained atoms (R2 = R - 0.5 Å, R3 = R + 0.5 Å)) on the N7...N2 and O6...N1 virtual bonds linking the neighboring guanines. LES simulations were usually followed by standard MD to allow the LES structure to locally relax. For further details about the protocol see ref 45.

Table 1. List of Simulations on $d(G_4T_4G_4)_2$ (Oxytricha) Quadruplex with Diagonal Loops

simulation name	initial structure	ion type[a]	trajectory length and type
		AMBER Simulations with parm99	
OXY^{NMR}	NMR	Na^+	10 ns MD
OXY	X-ray	Na^+	5 ns MD
OXY_K	X-ray	K^+	5 ns MD
OXY^{NMR}_LES	NMR	Na^+	6 ns LES
OXY^{NMR}_LES_MD	OXY^{NMR}_LES end	Na^+	3 ns MD
OXY_SPC_Kd	X-ray	K^+ ions (Dang), SPC waters	50 ns MD
		AMBER Simulations with parmbsc0	
OXY_bsc0_0	X-ray	Na^+	50 ns MD
OXY_bsc0_1	X-ray	Na^+	50 ns MD
OXY_bsc0_2	X-ray	Na^+	50 ns MD
OXY_bsc0_3	X-ray	Na^+	50 ns MD
OXY_bsc0_4	X-ray	Na^+	50 ns MD
OXY_bsc0_K2	X-ray	K^+ ions with radius of 2.4 Å	50 ns MD
OXY_bsc0_Kd	X-ray	K^+ ions (Dang)	50 ns MD
OXY_bsc0_hs_Kd	X-ray	excess salt 0.2 M KCl, K^+ ions (Dang)	50 ns MD
OXY_bsc0_hs_SPC_Kd1	X-ray	excess salt 0.2 M KCl, K^+ ions (Dang), SPC waters	50 ns MD
OXY_bsc0_hs_SPC_Kd2	X-ray	excess salt 0.2 M KCl, K^+ ions (Dang), SPC waters	50 ns MD
OXY_bsc0_Kc	X-ray	K^+ ions (Cheatham)	50 ns MD
OXY_bsc0_hs_Kc1	X-ray	excess salt 0.2 M KCl, K^+ ions (Cheatham)	50 ns MD
OXY_bsc0_hs_Kc2	X-ray	excess salt 0.2 M KCl, K^+ ions (Cheatham)	50 ns MD
OXY_bsc0_LES	X-ray	Na^+	20 ns LES
OXY_bsc0_LES_K2	X-ray	K^+ ions with radius of 2.4 Å	20 ns LES
OXY_bsc0_LES_MD	OXY_bsc0_LES end	Na^+	20 ns MD
OXY_bsc0_LES_MD_K2	OXY_bsc0_LES_K2 end	K^+ ions with radius of 2.4 Å	20 ns MD
		AMBER Simulations with Chi Modification + Either parm99 or parmbsc0	
OXY_chi	X-ray	Na^+	50 ns MD
OXY_bsc0_chi	X-ray	Na^+	50 ns MD
		CHARMm Simulations	
OXY_CHARMm	X-ray	standard CHARMm Na^+ ions	40 ns MD
OXY_CHARMm_mod	X-ray	Na^+ ions with radius of 1.16 Å	20 ns MD
OXY_CHARMm_K	X-ray	standard CHARMm K^+ ions	20 ns MD
PARA_CHARMm[b]	X-ray	standard CHARMm Na^+ ions	10 ns MD

[a] Net neutralizing set of standard AMBER cations and TIP3P water model if not stated otherwise. [b] Test simulation of parallel four-quartet guanine stem $d(G_4)_4$.[26]

MM-PBSA Free Energy Calculations. PB analysis was performed using a modified MM-PBSA procedure.[84,85] Both force field parameters (parm99 and parmbsc0) were employed for the MM part. The Cornell et al. (parm94) charge set, PARSE vdW radii,[108] and a dielectric constant of 1 for DNA were used. The Sander module of AMBER was used for MM energy terms, Delphi software[109] for PB contributions, and Molsurf for calculating SASA. The MD trajectories were examined in 10 ps intervals.

The MM-PBSA energy was calculated with an explicit inclusion of the channel cations (with Na^+ parameters adapted for the free energy computations) as in detail described elsewhere.[70] In order to obtain meaningful numbers for the trajectories in which one cation left the channel the closest solvent ion was considered as a part of the structure. We replaced potassium cations in particular trajectories with sodium cations as we wanted to obtain comparable results. (When attempting to use the potassium ion parameters, the resulting values were far away of the energy interval given by other structures). Since the MM-PBSA calculations are utilized only as a supplementary tool, we did not try to tune the K^+ parameters for free energy computations. MM-PBSA analysis was performed with parm99, also for the $d(G_4T_4G_4)_2$ MD trajectories that were produced with parmbsc0, and vice versa, i.e., we also cross-calculated free energies with the two force fields. The basic free energy trends are the same with both force fields.

CHARMm Simulations. The simulations were performed with the CHARMm code[110] using the CHARMm27 force field for nucleic acids.[81,82] The starting coordinates were the same as for the AMBER simulations. The equilibration protocol started with MD which was applied first to the water molecules only (5 ps) and then to the solvent (water + ions) (25 ps). Then the system was subjected to the several rounds of minimization with gradually reduced harmonic constraints on DNA. The final minimization was performed without any constraints. After that, the whole system was heated from 50 to 300 K in 30 ps by 50 K increments. The Particle Mesh Ewald (PME) method was used for treatment of electrostatic interactions.[101] MD simulations were run with a 2 fs time step and the SHAKE algorithm[102] to constrain all bonds to hydrogens. Two types of sodium ions were tested - either standard sodium ions (with radius 1.3638 Å and well depth 0.0469 kcal/mol) or modified (radius 1.163 Å and well depth 0.21 kcal/mol).[111] For potassium ion the following parameters were employed: radius of 1.7638 Å and well depth 0.0870 kcal/mol. As noted below, however, the results do not depend on these fine details of ion parametrization.

List of Simulations and Abbreviations. More than 1.5 μs of MD and LES trajectories (aggregated time) were run with the above-described protocols, with Na^+, K^+, or KCl ion atmospheres, considering various ion parameters and with

Table 2. List of Simulations on Human Telomere (HT) Quadruplex[15b]

abbreviation	initial structure	ion type[a]	trajectory length
	AMBER Simulations with parm99		
HT	X-ray	Na^+	10 ns MD
HT_K	X-ray	standard K^+	10 ns MD
HT_K2	X-ray	K^+ ions with radius of 2.4 Å	10 ns MD
HT_K3	X-ray	K^+ ions with radius of 2.5 Å	10 ns MD
	AMBER Simulations with parmbsc0		
HT_bsc0	X-ray	Na^+	40 ns MD
HT_bsc0_K2	X-ray	K^+ ions with radius of 2.4 Å	50 ns MD
HT_bsc0_hs_Kd	X-ray	excess salt 0.3 M KCl, K^+ ions (Dang)	50 ns MD
HT_bsc0_LES	X-ray	Na^+	20 ns LES
HT_bsc0_LES_K2	X-ray	K^+ ions with radius of 2.4 Å	20 ns LES
HT_bsc0_LES_MD	HT_bsc0_LES end	Na^+	20 ns MD
HT_bsc0_LES_MD_K2	HT_bsc0_LES_K2 end	K^+ ions with radius of 2.4 Å	20 ns MD
	AMBER Simulations with Chi Modification and Either parmbsc0 or parm99		
HT_chi	X-ray	Na^+	50 ns MD
HT_bsc0_chi	X-ray	Na^+	50 ns MD
HT_bsc0_bsc0+chi	HT_bsc0 end	Na^+	50 ns MD
HT_chi_ LES	X-ray	Na^+	20 ns LES
HT_bsc0_chi_ LES	X-ray	Na^+	20 ns LES
HT_chi_LES_MD	HT_chi_ LES	Na^+	20 ns MD
HT_bsc0_chi_LES_MD	HT_bsc0_chi_ LES	Na^+	20 ns MD
	CHARMm Simulations		
HT_CHARMm	X-ray	standard CHARMm Na^+ ions	10 ns MD
HT_CHARMm_K	X-ray	standard CHARMm K^+ ions	10 ns MD

[a] Net neutralizing set of standard AMBER cations and TIP3P water model if not stated otherwise. [b] In the abbreviations, if not specified otherwise, the simulations were run with parm99 and Na^+ ions. "bsc0", "chi", and "CHARMm" abbreviations indicate that parmbsc0, Ode et al., and CHARMm force fields were used. "LES" and "LES_MD" mean LES simulation and standard simulation that follows LES simulation, respectively. "K", "K2", and "K3" stand for simulations with K^+ having standard 2.66 Å, 2.4 Å, and 2.5 Å radii, respectively. Kc and Kd stand for Cheatham and Dang parameters of K^+ ions, and "hs" marks higher (excess) salt simulations.

five different force field variants. A list of trajectories and abbreviations is given in Tables 1 and 2.

These simulations are abbreviated as OXY or OXY^{NMR} for the X-ray[14] and NMR[30] starting structures. The X-ray structure has five integral potassium ions at the start (three channel and two stem-loop junction K^+). In the simulations with Na^+ ions, coordinates of structural K^+ ions were used for structural Na^+ ions. In the abbreviations, if not stated otherwise, the simulations were run with parm99 and net-neutralizing Na^+ ions. "bsc0", "chi", and "CHARMm" abbreviations indicate that parmbsc0, Ode et al., and CHARMm force fields were used. "LES" and "LES_MD" mean LES simulation and standard simulation that follows LES simulation, respectively. "K", "K2", and "K3" stand for simulations with K^+ having standard 2.66 Å, 2.4 Å, and 2.5 Å radii, respectively. "hs" marks higher (excess) salt simulations, and Kc and Kd stand for Cheatham and Dang parameters of K^+ ions.

Results

Simulations of the $d(G_4T_4G_4)_2$ Quadruplex from Oxytricha (OXY Quadruplex) with Diagonal Loops. *Description of the Structure.* The antiparallel four-quartet bimolecular quadruplex consists of two $d(G_4T_4G_4)$ strands and has two diagonal four-thymidine loops (T5-T6-T7-T8 and T17-T18-T19-T20) - see Figure 1b. Both loops are nearly identical in the X-ray structure[14] with mutual heavy atom rmsd = 0.21 Å. The first and third thymines in each loop are coplanar and connected by T5(O2)...T7(N3) (3.09 Å) and T17(O2)...T19(N3) (2.99 Å) H-bonds, respectively. A notable feature is the presence of K^+ at each stem-loop junction, so that there are three stem (channel) and two stem-loop junction (channel entrance) cations present in the experimental structure. The stem-loop junction ions are coordinated to four O6 atoms of the outer quartet guanines and two O2 atoms of the adjacent thymine basepair (either T5&T7 or T17&T19). This X-ray structure is except for details that are not significant for the simulations in full agreement with other available relevant X-ray[78] and NMR structures.[30,88] Since the experimental top and bottom loops have basically identical topologies, each simulation provides two independent loop trajectories.

Behavior of the Stem in AMBER Simulations. The parm99 force field provides a good description of the G-DNA stem, as consistently shown in all our preceding studies and confirmed also by others (see the Introduction for more details). Good performance of the force field for the stem is confirmed also in the present study and will not be further discussed. Parmbsc0 also provides satisfactory description of the G-DNA stem. We did not make a detailed analysis of the parm99 vs parmbsc0 dynamics of the stem, as no major problems with the stem are indicated.

Redistribution of the Ions. Several earlier conventional 5−10 ns parm99 MD simulations of $d(G_4T_4G_4)_2$ show basically stable loop trajectories.[45] However, the stem-loop junction ions were lost (when initially present) within a very few ns and were not replaced by other bulk ions. In this study we analyze twenty-four 5−50 ns simulations with initially five ions associated with the $d(G_4T_4G_4)_2$ quadruplexes (Table S1). Irrespective of which solute and ion force field parameters were used, the initial experimental configuration with five integral G-DNA ions is unstable. In the

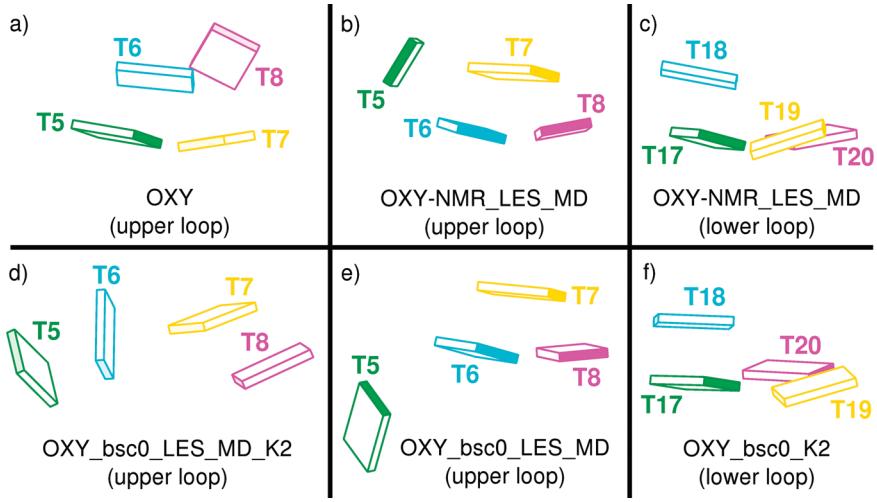

Figure 3. Experimental and three key computed structures of the diagonal four thymidine loops of the Oxytricha quadruplex. a) The experimental structure, b) and c) two LES geometries with parm99, d) entirely unfolded LES geometry with parmbsc0 obtained in one simulation, e) parmbsc0 LES geometry resembling the parm99 LES structure in b), and f) restructured loop in standard parmbsc0 simulation similar to the LES predicted topology in c). Green - T5, T17; cyan - T6, T18; yellow - T7, T19; magenta - T8, T20. Structures c) and f) appear to be achieved by a vast majority of AMBER simulations where the length of the simulation is sufficient to see a transition.

vast majority of simulations, including excess-salt KCl simulations, both stem-loop junction ions left the structure within a very few ns. They were not replaced by any other ion from the bulk or stem channel while three ions remained in the stem (except of one CHARMm simulation, where only two ions remained associated with the quadruplex). In very few simulations an ion was still residing at the end of the simulation in the stem-loop junction position. However, in these cases only three or four ions remained associated with the G-DNA (its central channel area). Therefore, the number of ions was reduced, specifically in the stem cavity adjacent to that bound junction cation. Since the stem-loop junction ions are coordinated also to the outer quartets, it is not surprising that upon reduction of the number of bound cations to less than five some of them can reside in the stem-loop junction. They then provide primary stabilization of the outer quartet. This resembles binding of two ions to the two-quartet stem of thrombin binding aptamer quadruplex, where two K^+ ions are expected to bind to the quartets from the loop area while keeping the central cavity empty.[112]

It is not easy to pinpoint the exact origin of this imbalance in force field description of cation−DNA interaction. It may reflect the underestimation of the direct cation - solute interactions illustrated in Figure 2 (note that the ions are parametrized to provide correct ion-solvation energies, not cation-nucleobase interaction energies) or an overestimation of the ion - ion repulsion. Perhaps the ions in the experimental structure may be stabilized due to rigidification of the experimental X-ray structure or some crystal packing effects. However, it is difficult to believe that this can fully explain the discrepancy between theory and experiment. We can conclude that presently the experimental ion binding to $d(G_4T_4G_4)_2$ cannot be reproduced by simulations.

Loop Structures. As noted above, for the $d(G_4T_4G_4)_2$ quadruplex, the diagonal loop structures were basically stable in earlier standard short simulations with parm99 (Figure 3a), but they were lost in LES simulations with the same force field.[45] The LES-MD structure changed the positions of thymines entirely and formed two new H-bonds in the upper loop, T6(N3)...T8(O4) and T6(O2)...T8(N3), with stacking between the T6...T8 base pair and T7 (Figure 3b). In the second loop rearrangement (Figure 3c) the original base pair is lost, and a new interaction between T17 and T20 is formed with only a single T17(N3)...T20(O4) H-bond. In addition, the methyl groups of T18 and T20 contacted the O2 atom of T17 due to a coplanar arrangement of these three bases - see ref 45 and Figure 3c.

We have thus performed two LES simulations with parmbsc0 (four independent loop trajectories) in which all loops lost their X-ray geometries, similar to the earlier parm99 results. The parmbsc0 LES simulations are much longer than the parm99 LES simulations, and the loops still show no attempts to return to the experimental structure. One loop in the **OXY_bsc0_LES_K2** simulation became completely unfolded (Figure 3d). The three other LES-simulated loops were completely restructured, with the final structures clearly resembling the earlier parm99 LES geometries. Actually, the parmbsc0 and parm99 results are strikingly similar (Figure 3) although the unfolded loop geometry (Figure 3d) was not seen with parm99. However, the parm99 LES simulation was short. Thus, parm99 and parmbsc0 LES data are mutually consistent for the $d(G_4T_4G_4)_2$ loops.

In standard simulations, we concentrated on the parmbsc0 force field, as parm99 was invalidated due to its troubles in B-DNA simulations, rendering parmbsc0 the only AMBER force field that can be used for DNA systems.[79] Our thirteen parmbsc0 simulations gave an unprecedented set of 26 independent 50 ns loop trajectories. Eighteen of them were basically stable with small fluctuations of top thymines (either T8 or T20). In the remaining cases we evidenced formation of a "triadlike" structure in which the top thymine (T8 or T20) formed a close-to-planar arrangement with the original T...T base pair in the particular loop (Figure 3f). This arrangement once formed is stable and clearly resembles the

Table 3. MM-PBSA Free Energy (see Method) in kcal/mol, Averaged over 1−5, 21−25, and 46−50 ns Trajectory Portions

MD simulation	1−5 ns	21−25 ns	46−50 ns
OXY_bsc0_0	−5053 ± 20	−5054 ± 19	−5052 ± 20
OXY_bsc0_1	−5054 ± 20	−5055 ± 20	−5051 ± 20
OXY_bsc0_2	−5050 ± 20	−5054 ± 19	−5050 ± 20
OXY_bsc0_3	−5054 ± 21	−5046 ± 21	−5052 ± 19
OXY_bsc0_4	−5052 ± 20	−5050 ± 19	−5053 ± 20

LES topology shown in Figure 3c. It is the same substate. This suggests that the simulations are slowly converting to different but characteristic geometry, which was anticipated by LES calculations.

Parmbsc0 simulations with standard sodium ions provided us with stable loop structures in almost all cases. Ion modifications in other simulations (see Table 1) were associated with a loss of experimental geometry in 40% of cases. Excess salt simulations with Dang ion parameters kept both loop geometries stable, while Dang ion setting in net-neutralizing salt conditions lost both of them. All three simulations with Cheatham ion parameters showed a formation of "triadlike" structures in one of the loops. However, consideration of these individual cases is not statistically significant and the behavior is most likely incidental. Note (see above) that the modified ion conditions do not stabilize the arrangement with five integral ions in the structures. Table S2 summarizes development of all backbone torsions of both loops in most $d(G_4T_4G_4)_2$ simulations, which gives more detailed insight into the trajectories.

MM-PBSA was used to investigate the energetic origin of the conformational transitions found along some trajectories. However, results summarized in Table 3 for 5 trajectories (four without transition and one with a loop transition; **OXY_bsc0_1**) fail to detect any consistent, statistically significant change in the free energy of the system, which seems quite well converged irrespective of whether or not conformational transitions occur along the trajectory. Thus, the expected free energy change associated with the change of the loop topology appears to be below the threshold which could be detected by MM-PBSA with a confidence, and accordingly the use of MM_PBSA to discriminate between different structural families is not recommended in this particular case.

Supporting Information Tables S4 and S5 contain MM_PBSA data for some other trajectories. The data also do not seem to suggest any easy way to monitor the change of the loop structures by the approximate free energy calculations. Specifically, the free energy of the **OXY_bsc_LES_MD** simulation where both loops are rearranged (−5050 kcal/mol at the end of the standard simulation following the LES run) remains within the range of values in the Table 3, i.e., is not visibly improved. Therefore, we do not use the MM_PBSA data to reach any conclusions in this study (we rely purely on the structural data), and we plan to attempt a more thorough free energy analysis in some subsequent work.

Chi Modification of Force Field. The modification of the AMBER force field by Ode et al.[80] was combined with both parm99 and parmbsc0. We have carried out two 50 ns standard simulations in which the loops were stable and looked stiffer than in parm99 and parmbsc0 standard simulations. Stacking interactions and H-bonds in the loops are all stable. There were perhaps marginally better values of rmsd in the simulated structures with respect to the X-ray structure when we compare **OXY_chi** vs **OXY** and also **OXY_bsc0_chi** vs **OXY_bsc0** simulations (Figure S1).

We did not attempt further simulations for the following reasons. Our simultaneous test simulations (not shown) of B-DNA and Sarcin Ricin 23S rRNA internal loop with the Ode et al. parametrization did not change the results substantially (including the χ angle and helical twist in B-DNA) compared to parmbsc0 (and parm99 for the RNA) simulations. However, the simulated molecules appeared again visually stiffer. The overall impression so far is that the χ-modification apparently slows down transitions (some backbone substates, e.g,, if present) but does not change the ultimate conformational preference. Therefore, it is not surprising that the simulations with modified χ did not reveal any substantial changes of the $d(G_4T_4G_4)_2$ which even with parmbsc0 and parm99 take a time. Meanwhile we obtained better insights into the performance of this force field using the HT G-DNA simulations (see below) and decided that further simulations of $d(G_4T_4G_4)_2$ with the Ode et al. force field are not needed.

Molecular Dynamics with CHARMm. All CHARMm simulations (cf. Table 1) resulted in loop structures that do not resemble the experimental ones. Almost no structural features were kept, including the thymine base pairs and stacking interactions (Figures S2 and S3). Rmsd values were high (Figure S2). During the CHARMm simulations the loops adopted two main conformations (Figure S4). The first conformation is characterized by stacking interactions between T5 and T6 (upper loop) or T17 and T18 (lower loop). In the second conformation T5 stacks on T8 (upper loop) or T17 stacks on T20 (lower loop). Notable is that with CHARMm simulations the X-ray loop structures were lost in standard simulations. In one of the simulations only two ions remained in the channel, while in the other two simulations there were two ions in the stem channel and one ion coordinated to the outer quartet from the loop region (Table S1). This indicates that even the stem behavior is not fully perfect. Therefore, we have carried out a test simulation of an all-parallel four quartet G-DNA stem with CHARMm with Na^+ (last simulation in Table 1). The simulation lost one of the stem ions rather quickly, which was never observed in analogous AMBER simulations (Figure S5). This behavior is not promising, especially when considering that we have used Na^+ cations which should have no steric problems within the stem.

Simulations of the Human Telomeric Monomolecular d[AGGG(TTAGGG)$_3$] Quadruplex (HT Quadruplex) with Propeller Loops. *Description of the Structure.* The structure consists of a common three-quartet guanine stem with two ion cavities and three similar thymine−thymine−adenine propeller loops (T5-T6-A7, T11-T12-A13, and T17-T18-A19) - see Figures 1c and 4. In each loop the adenine is sandwiched between the two thymines but stacks primarily with the first thymine, i.e., there are stacking interactions

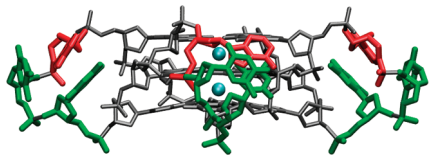

Figure 4. The crystal structure of d[AGGG(TTAGGG)$_3$] (HT) quadruplex; side view. Cyan dots are the channel K^+ ions; loop nucleotides are shown using green (thymine) and red (adenine) licorice model.

between T5 and A7, T11 and A13, and T17 and A19. The other thymines (T6, T12, and T18) are unstacked.

As the loops are conformationally restricted, their backbone torsion angles differ from the canonical DNA α/γ g-/g+ conformation. The first thymine in each loop shows α/γ values of g+/t. The second thymine has α/γ torsions roughly in t/g+ position while the adenine is in the canonical g-/g+ region. Note that the α/γ g+/t substate of the first nucleotides in each loop is the same torsion combination which had to be penalized in the parmbsc0 force field to stabilize B-DNA simulations.[79]

Standard Molecular Dynamics with parm99 Force Field. Guanine stem was stable when simulated with Na^+ and both its channel cations stayed inside the structure. However, with the standard K^+ ion parameters one of the cations left the channel. This most likely is caused by the imbalance in description of solute - cation interactions as described in detail in the Method section. Thus for further simulations we reduced the K^+ radius (see the Method section for further explanation). This stabilized the stem but did not stabilize the loops (see Table 2 for the list of all HT simulations).

Standard MD simulations with the parm99 force field were not capable of keeping the experimental loop structures even on a 10 ns scale, irrespective of the cation parameters. The simulations resulted in a mixture of diverse loop structures, none of them resembling the experiment. Loop geometries were unfolded, and base stacking and other structural signatures of the experimental loops were lost (cf. Figure 5a,b). The loops were swiftly diverging to very diverse conformations, while the experimental one has never been sampled again (see further details in the Supporting Information, including Table S3 summarizing changes of loop backbone angles in all HT simulations). For this reason it was not necessary to make longer simulations or to attempt LES.

Standard Molecular Dynamics and LES Simulations with parmbsc0. In standard parmbsc0 simulations, all three propeller loop structures remained quite close to the experiment even after 50 ns long runs (Figure 5c) and adopted essentially identical geometries. Nevertheless, the agreement with experiment is not perfect for two reasons. The adenine changes its stacking thymine partner from T5 to T6, and the γ trans topology of the first thymine is lost (Figure 6, Table S3).

The loss of the γ trans of the first loop nucleotide is in fact not surprising. Parmbsc0 stabilizes the canonical conformation of α/γ torsional angles compared to g+/t, relative to parm99.[79,113] This is an absolute requirement to achieve stable B-DNA simulations. However, in the HT quadruplex X-ray structure, the first thymine of all three loops (T5, T11, and T17) has γ trans accompanied with the corresponding α torsion in g+. This arrangement was not stable with parmbsc0 simulations (see Figure 6) with both ion types and the backbone flipped basically to the canonical α/γ combination. Some of the loops switched their first thymine to the canonical region quickly; in a few cases it took ~20 ns, but at the end of the standard simulations all nine independent loops (three simulations including one excess-salt, see Tables 2 and S3) lost the γ trans. On the other hand, the remaining loop nucleotides were stabilized by the parmbsc0 force field, sharply contrasting the parm99 behavior. It thus appears that, regarding simulation of this particular loop, the parmbsc0 force field is slightly too canonical though definitely improved over parm99. It allows a quite satisfactory description of this particular loop. At first sight, these simulations might indicate that the α/γ correction of parmbsc0 could be reduced. However, based on the experience accumulated while working on the g+/t B-DNA problem, any significant weakening of the γ trans correction would likely undermine the B-DNA simulations. Note also that (see above) this would hardly improve the loop behavior of the OXY quadruplex where both parm99 and parmbsc0 appear to provide practically identical results.

The modest rearrangement of the loops in parmbsc0 simulations further included creation of a new hydrogen bond between O4 of the first thymine in each loop and a guanine amino group of the central quartet of the stem. The structural change of base stacking in the loops was a consequence of the backbone flip. When the γ torsion flipped from t to g+ value, the α torsion left the g+ arrangement and after some fluctuations adopted a value of ca. $-120°$. This flip brought the above-noted hydrogen bond donors and acceptors close to each other, and the new H-bond was formed. Reduction of the distance between the involved atoms from the starting T(O4) - G(H22) value of 7 Å to the final value <2 Å resulted also in the change of base stacking in the loops. While in the X-ray structure the adenine stacked with the first thymine in each loop, in the final loop structures the adenine stacked with its neighboring thymine in the loop, because the first thymine was rotated and bound to the stem via the newly formed H-bond. All three changes (backbone flip, stacking change, and H-bond formation) appear to be interrelated and in a delicate balance.

Results of excess-salt simulation with Dang parameters for ions are the same as in other parmbsc0 simulations. We again evidenced restacking of the loops, creation of H-bonds between O4 atoms of thymine bases and guanine amino groups of the central quartet of the stem and the loss of γ trans. Thus changing the salt condition is not affecting the simulation outcome significantly, as usual with nucleic acids simulations.[114]

As parmbsc0 provided a rather satisfactory loop description, we performed also extensive LES simulations. LES confirmed that for this loop the parmbsc0 force field is not far from the target structure since the LES simulations localized similar geometries as the standard simulations. The above-mentioned H-bonds between O4 atoms of thymine

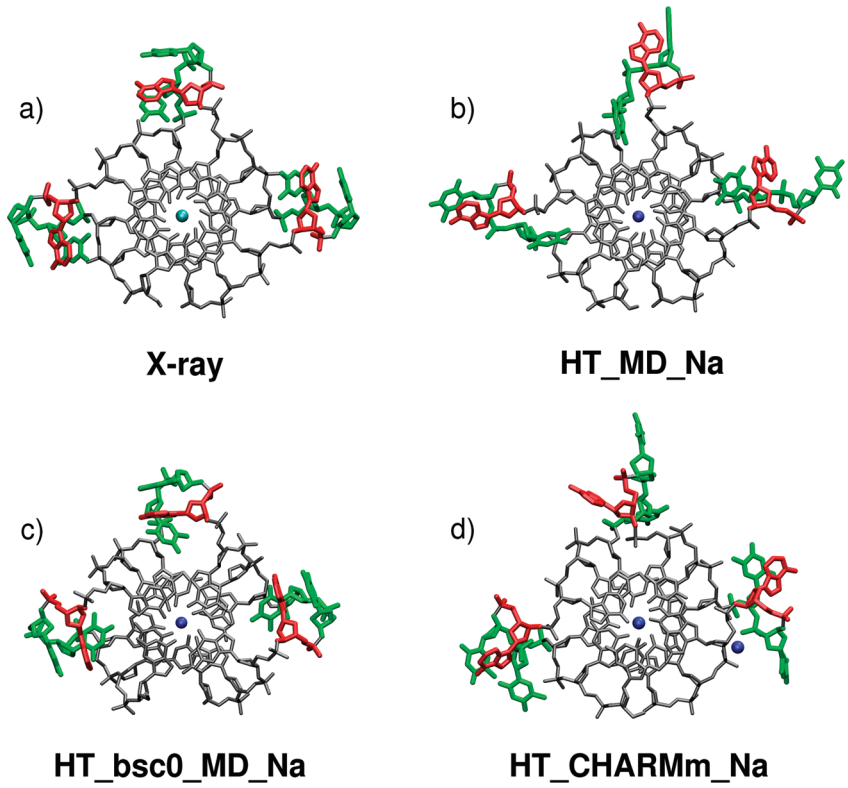

Figure 5. Experimental and simulated structures of the human telomeric quadruplex a) the X-ray structure, b) the structure from parm99 HT simulation, c) the structure from HT_bsc0 simulation, and d) the structure from the HT_CHARMm simulation. Cyan and blue dots are the channel K^+ and Na^+ ions, respectively; loop nucleotides are shown using a green (thymine) and red (adenine) licorice model. Note that in part d) one of the ions left the channel and is seen trapped in the loop region far from the channel. MD structures were averaged over the last 0.5 ns of the trajectory (except for the lost ion in part d).

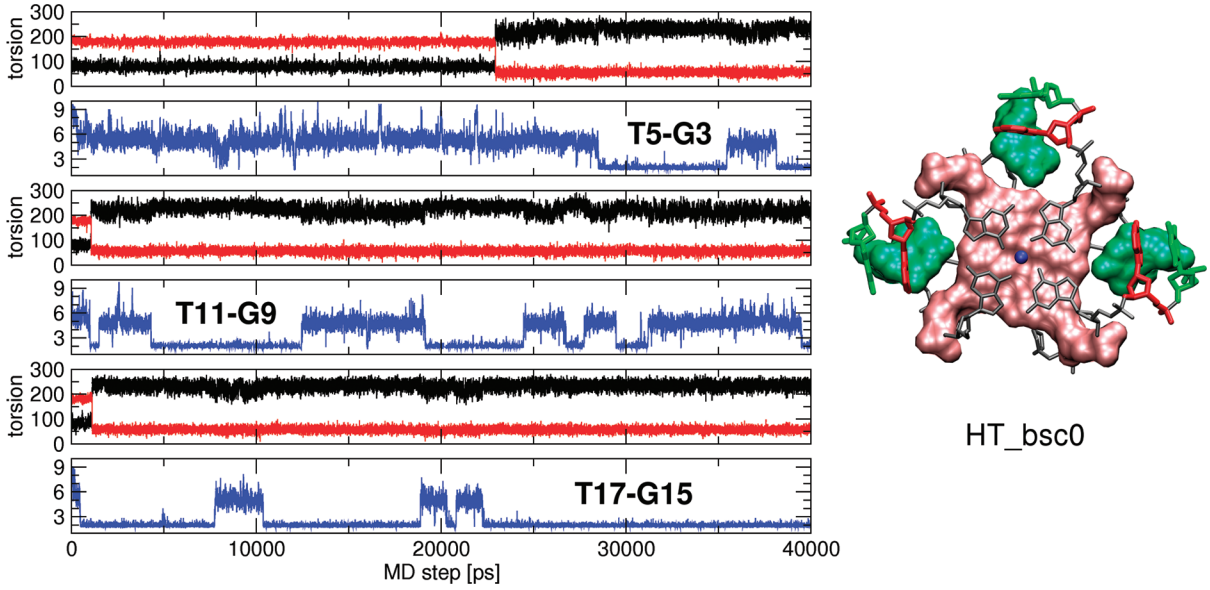

Figure 6. Simulation HT_bsc0 with parmbsc0. a) Time development of α and γ torsions and the loop - stem H-bond of the first thymine in each loop, i.e. T5, T11, and T17. Each pair of graphs corresponds to one loop; the upper graph shows α (black) and γ (red) torsions; the lower graph shows the H-bond between the thymine and the guanine stem. Note that two γ trans states are lost swiftly, the remaining one after more than 20 ns. b) Averaged (last 0.5 ns) structure of HT_bsc0 simulation. The middle guanine quartet and the first thymines in each loop are highlighted by space filling representation.

bases and guanine amino group of the central quartet of the stem were not stably formed within both LES trajectories (**HT_bsc0_LES** and **HT_bsc0_LES_K2**). The **HT_bsc0_LES** trajectory even exhibited the smallest rmsd from all of the trajectories compared to the X-ray structure. Some loops had still γ of the first nucleotide in trans at the end of the LES run. However, the subsequent standard MD trajectories aimed to relax the LES structures show basically again formation of the structure seen in the standard simulations with the H-bonds between the first thymines of the loops

and the stem. The LES simulations give an impression that the parmbsc0 force field prefers the new loop topology as the true global minimum while still sometimes attempting to regain some of the features of the original structure.

Chi Modification of the AMBER Force Field. Simulations run with modified parameters for χ torsions did not bring any breakthrough. The 50 ns **HT_bsc0_chi** simulation resulted in a structure very similar to the **HT_bsc0** simulation. The γ trans of the first thymines in each loop is lost, adenines change their stacking thymine partners, and H-bonds between the first thymine in loop and guanine of the middle quartet are formed. As we noted above, the χ modification appears to rigidify the simulated molecule while not affecting the structures that result from transitions. I.e., we see the same development as without the χ correction, albeit on a longer time scale. The ultimate outcome of the simulation is dictated by whether the χ modification is combined with parm99 or parmbsc0. Even the χ angle values achieved in the simulations with χ modification appear to be unaffected by the χ modification. The modification appears to change the torsional profile mainly in the region between anti and syn nucleotide geometries, which could affect the kinetics and path of the anti to syn transitions; however, further tests will be needed to obtain more insights. When the χ correction was combined with parm99, the loops were significantly destabilized, again as inherent to the parm99 force field without the χ correction. We further took the final structure from **HT_bsc0** simulation, added χ modification and run additional MD. After 50 ns the structure was not changed, and not a single first thymine in the loops switched back to trans. One loop was slightly closer to the original X-ray structure as the H-bond between thymine and guanine was broken, but this is an insignificant observation. In summary, while the χ correction slows down transitions, we see that all simulations are progressing to the same structures as those obtained either with parmbsc0 or parm99 without χ modification, depending on which of them is combined with the χ correction. Therefore, so far we do not see any advantage of using the χ correction, which is also supported by our B-DNA and Sarcin Ricin RNA simulations (unpublished data).

Molecular Dynamics with CHARMm. With the CHARMm force field, the loop geometries appeared as unstable as with parm99, that means in entire disagreement with the experiment and not converging to any common structure (Figure 5d). Thus we do not provide detailed analyses. Even the stem behavior was imperfect. One of the two integral cations left the stem channel at ~2 and ~3 ns for the Na^+ and K^+ simulations, respectively. Such behavior was sometimes observed with AMBER and standard K^+ ions (see Method for discussion) due to the exaggerated short-range repulsion. However, channel ion instability with AMBER has never been seen using a smaller radius for K^+ and any of the Na^+ parameters. The swift loss of the channel ions in CHARMm simulations (already seen for CHARMm OXY and parallel quadruplex, see above) is definitely in disagreement with experiments, and thus no further simulations were attempted.

Discussion and Conclusions

We have carried out an extensive set (more than 1.5 μs in total) of simulations of two guanine quadruplex DNA (G-DNA) molecules: the $d(G_4T_4G_4)_2$ dimeric quadruplex with diagonal loops[14] and also the parallel stranded human telomeric monomolecular quadruplex d[AGGG(TTAGGG)$_3$] with three propeller loops,[15] as revealed by X-ray crystallography. The main aim of the study was to analyze the capability of the explicit solvent molecular dynamics (MD) technique to describe the complicated single stranded loop topologies of these G-DNA molecules.

We have tested five force fields: the parm99 AMBER force field,[74] its recent reparametrization aimed to stabilize B-DNA known as parmbsc0,[79] a combination of both parm99 and parmbsc0 with modification of the χ torsional profile suggested by Ode et al.,[80] and the CHARMm force field[81,82] for nucleic acids. In addition, several ion parameters were used, and net-neutralizing simulations were compared with excess salt ones. The loop behavior does not appear to be dependent on the type of ions, and also the excess salt does not appear to affect the solute behavior on the present time scale. Besides standard simulations, we applied also extensive runs of locally enhanced sampling (LES) dynamics,[76] which is designed to improve sampling of the loop regions, in order to overcome limitations of the short time scale of the simulations. The LES simulations nicely complement the picture emerging from long standard simulations. We see a basic agreement between LES and MD results for both quadruplexes. The study confirms that single stranded hairpin loop topologies represent a major problem for molecular mechanical force fields and that much caution and validation against experimental data is necessary before accepting as real trajectories obtained for these systems.

The $d(G_4T_4G_4)_2$ quadruplex contains, besides the three genuine binding sites for cations in the channel of its stem, also ion binding site at each stem-loop junction. This arrangement of five cations in the quadruplex core region is entirely unstable in all simulations. Most simulations ended up with just three cations in the stem cavities, while there was not a single simulation with five ions inside the structure at the end. The diagonal loops in this structure are stable in short AMBER simulations (all force field variants), while they are lost in CHARMm simulations. In longer AMBER simulations, however, the loops start to convert to a substantially different arrangement, as seen in Figure 3c,f. Analysis of standard and LES simulations give a clear indication that parm99 and parmbsc0 have similar performance for this loop.

The propeller loops of d[AGGG(TTAGGG)$_3$] are very unstable in standard simulations with parm99 and CHARMm, resulting in a diverse mixture of incorrect geometries. Parmbsc0 provides a substantially better description of the -TTA- propeller loops, albeit there are some differences compared with the experimental structure. Namely, γ trans of the first thymine in each loop is lost. This is not surprising, as this force field has been parametrized to penalize γ trans

in order to stabilize B-DNA simulations.[79,113] This also results in some change of stacking partners in the loop. Despite that, this geometry is obtained reproducibly and partially resembles the experimental one.

It is to be noted that the characteristic loop topology of $d(G_4T_4G_4)_2$ which is not reproduced by the force fields has been unambiguously determined by X-ray and solution experiments, with different ion conditions and also with different crystal packing environments.[14,30,78,88] On the other hand, it is well established that the d[AGGG(TTAGGG)$_3$] HT quadruplex would likely fold to an entirely (globally) different topology with an antiparallel (instead of parallel) stem in the presence of Na^+ in solution,[115] as it can adopt multiple topologies. However, this to our opinion is not related to the instability of the loops in our simulations. The overall topological variability in the experiments reflects free energy balance between very different folds. Once a ns-scale simulation starts from one of these folds (parallel with propeller loops in our case) its outcome should not be affected by the fact that some other topology would be more stable. The other topologies are entirely unreachable on the simulation time scale and thus do not interfere with the simulation outcome. The stem would have to be unfolded and refolded to form the alternative topologies. Therefore, once the simulation is confined within a given overall folding arrangement, the simulation should be capable of localizing the appropriate loop geometry provided the force field is appropriately balanced.

The modification of the AMBER glycosidic torsion by Ode et al. does not seem to bring any substantial change of the force field. Its most characteristic feature is rigidification of the simulated structures that slows down the transitions. That is, we see the same development as without the χ correction, albeit on a longer time scale. The ultimate outcome of the simulation is dictated by whether the χ modification is combined with parm99 or parmbsc0. No clear advantage appears then from using Ode's parameters, and the extra rigidification of the system is expected to produce undesired equilibration problems and potential error in the description of the flexibility pattern.

We suggest that the struggle of the force field to deal with the loops is not surprising. Their geometry is a result of a delicate balance of a large number of diverse competing forces including various noncanonical H-bonds between loop bases, different stacking options, specific ion interactions (see the OXY quadruplex), unusual backbone conformations, structural communication between stem and loop not only through the covalent linkage but also via H-bonds or ion interactions, complex solvation effects, and maybe some others. It appears to be very difficult to simultaneously balance all these diverse contributions to obtain the correct loop geometry. It is important to underline that the loops represent a daunting task for the MD simulation technique, and problems of the method with this specific type of nucleic acids architecture does not rule out successful application of the technique to most other types of nucleic acids molecules where it is much easier to obtain a sufficient balance of all the energy contributions. Overall our calculations demonstrate the need for a fine benchmarking of nucleic acids force fields outside from regular structures and well-defined compact arrangements. Ion parameters need to be included in these benchmarks, since for some of these structures they can play a key stabilizing role. Future generation force fields, including polarization corrections,[116,117] might be able to capture the behavior of these complex systems, but, in the meantime, careful checking of simulations in unusual structures such as the quadruplex loops seems necessary to avoid reaching erroneous conclusions.

Acknowledgment. This work was supported by the Ministry of Education of the Czech Republic [grants MSM0021622413 and LC06030], by the Grant Agency of the Academy of Sciences of the Czech Republic [grant numbers 1QS500040581 and IAA400040802], and by grant GA203/09/1476, Grant Agency of the Czech Republic. This work was also supported by the Academy of Sciences of the Czech Republic, grants no. AV0Z50040507 and AV0Z50040702, and by the Spanish Ministry of Science (BIO2006-01602 and Escience consolider Project). J. Sarzyñska acknowledges an access to the Poznań Supercomputing and Networking Centre.

Supporting Information Available: RMSd plots of selected MD simulations of OXY quadruplex, final structures and representative loop geometries of OXY quadruplex from CHARMm simulations, dynamics of channel ions in CHARMm simulations of all-parallel G-DNA stem, table of redistribution of cations in OXY quadruplex simulations, tables of important loops torsion angles for OXY and HT quadruplexes, and tables of free energy estimations for OXY and HT quadruplexes. This material is available free of charge via the Internet at http://pubs.acs.org.

References

(1) Burge, S.; Parkinson, G. N.; Hazel, P.; Todd, A. K.; Neidle, S. Quadruplex DNA: sequence, topology and structure. *Nucleic Acids Res.* **2006**, *34*, 5402–5415.

(2) Neidle, S.; Parkinson, G. N. The structure of telomeric DNA. *Curr. Opin. Struct. Biol.* **2003**, *13*, 275–283.

(3) Mergny, J. L.; Mailliet, P.; Lavelle, F.; Riou, J. F.; Laoui, A.; Helene, C. The development of telomerase inhibitors: the G-quartet approach. *Anti-Cancer Drug Des.* **1999**, *14*, 327–339.

(4) Neidle, S.; Read, M. A. G-quadruplexes as therapeutic targets. *Biopolymers* **2000**, *56*, 195–208.

(5) Huppert, J. L. Hunting G-quadruplexes. *Biochimie* **2008**, *90*, 1140–1148.

(6) Alberti, P.; Bourdoncle, A.; Sacca, B.; Lacroix, L.; Mergny, J. L. DNA nanomachines and nanostructures involving quadruplexes. *Org. Biomol. Chem.* **2006**, *4*, 3383–3391.

(7) Davis, J. T. G-quartets 40 years later: From 5′-GMP to molecular biology and supramolecular chemistry. *Angew. Chem., Int. Ed.* **2004**, *43*, 668–698.

(8) Hardin, C. C.; Perry, A. G.; White, K. Thermodynamic and kinetic characterization of the dissociation and assembly of quadruplex nucleic acids. *Biopolymers* **2000**, *56*, 147–194.

(9) Huppert, J. L. Four-stranded nucleic acids: structure, function and targeting of G-quadruplexes. *Chem. Soc. Rev.* **2008**, *37*, 1375–1384.

(10) Lane, A. N.; Chaires, J. B.; Gray, R. D.; Trent, J. O. Stability and kinetics of G-quadruplex structures. *Nucleic Acids Res.* **2008**, *36*, 5482–5515.

(11) Lane, A. N.; Jenkins, T. C. Structures and properties of multistranded nucleic acids. *Curr. Org. Chem.* **2001**, *5*, 845–869.

(12) Mergny, J. L.; De Cian, A.; Ghelab, A.; Sacca, B.; Lacroix, L. Kinetics of tetramolecular quadruplexes. *Nucleic Acids Res.* **2005**, *33*, 81–94.

(13) Paramasivan, S.; Rujan, I.; Bolton, P. H. Circular dichroism of quadruplex DNAs: Applications to structure, cation effects and ligand binding. *Methods* **2007**, *43*, 324–331.

(14) Haider, S.; Parkinson, G. N.; Neidle, S. Crystal structure of the potassium form of an Oxytricha nova G-quadruplex. *J. Mol. Biol.* **2002**, *320*, 189–200.

(15) Parkinson, G. N.; Lee, M. P. H.; Neidle, S. Crystal structure of parallel quadruplexes from human telomeric DNA. *Nature* **2002**, *417*, 876–880.

(16) Aboulela, F.; Murchie, A. I. H.; Lilley, D. M. J. NMR-study of parallel-stranded tetraplex formation by the hexadeoxynucleotide d(TG_4T). *Nature* **1992**, *360*, 280–282.

(17) Balagurumoorthy, P.; Brahmachari, S. K. Structure and stability of human telomeric sequence. *J. Biol. Chem.* **1994**, *269*, 21858–21869.

(18) Bardin, C.; Leroy, J. L. The formation pathway of tetramolecular G-quadruplexes. *Nucleic Acids Res.* **2008**, *36*, 477–488.

(19) Crnugelj, M.; Hud, N. V.; Plavec, J. The solution structure of d$(G_4T_4G_3)_2$: a bimolecular G-quadruplex with a novel fold. *J. Mol. Biol.* **2002**, *320*, 911–924.

(20) Dai, J. X.; Carver, M.; Yang, D. Z. Polymorphism of human telomeric quadruplex structures. *Biochimie* **2008**, *90*, 1172–1183.

(21) Gabelica, V.; Rosu, F.; Witt, M.; Baykut, G.; De Pauw, E. Fast gas-phase hydrogen/deuterium exchange observed for a DNA G-quadruplex. *Rapid Commun. Mass Spectrom.* **2005**, *19*, 201–208.

(22) Gros, J.; Rosu, F.; Amrane, S.; De Cian, A.; Gabelica, V.; Lacroix, L.; Mergny, J. L. Guanines are a quartet's best friend: impact of base substitutions on the kinetics and stability of tetramolecular quadruplexes. *Nucleic Acids Res.* **2007**, *35*, 3064–3075.

(23) Ida, R.; Wu, G. Direct NMR detection of alkali metal ions bound to G-quadruplex DNA. *J. Am. Chem. Soc.* **2008**, *130*, 3590–3602.

(24) Kettani, A.; Bouaziz, S.; Gorin, A.; Zhao, H.; Jones, R. A.; Patel, D. J. Solution structure of a Na cation stabilized DNA quadruplex containing G.G.G.G and G.C.G.C tetrads formed by G-G-G-C repeats observed in adeno-associated viral DNA. *J. Mol. Biol.* **1998**, *282*, 619–636.

(25) Phan, A. T.; Modi, Y. S.; Patel, D. J. Two-repeat Tetrahymena telomeric d(TGGGGTTGGGGT) sequence interconverts between asymmetric dimeric G-quadruplexes in solution. *J. Mol. Biol.* **2004**, *338*, 93–102.

(26) Phillips, K.; Dauter, Z.; Murchie, A. I. H.; Lilley, D. M. J.; Luisi, B. The crystal structure of a parallel-stranded guanine tetraplex at 0.95 angstrom resolution. *J. Mol. Biol.* **1997**, *273*, 171–182.

(27) Rosu, F.; Gabelica, V.; Houssier, C.; Colson, P.; De Pauw, E. Triplex and quadruplex DNA structures studied by electrospray mass spectrometry. *Rapid Commun. Mass Spectrom.* **2002**, *16*, 1729–1736.

(28) Sket, P.; Crnugelj, M.; Kozminski, W.; Plavec, J. 15NH_4^+ ion movement inside d$(G_4T_4G_4)_2$ G-quadruplex is accelerated in the presence of smaller Na^+ ions. *Org. Biomol. Chem.* **2004**, *2*, 1970–1973.

(29) Sket, P.; Crnugelj, M.; Plavec, J. Identification of mixed dication forms of G-quadruplex in solution. *Nucleic Acids Res.* **2005**, *33*, 3691–3697.

(30) Smith, F. W.; Feigon, J. Quadruplex structure of Oxytricha telomeric DNA oligonucleotides. *Nature* **1992**, *356*, 164–168.

(31) Zhou, J.; Yuan, G.; Liu, J. J.; Zhan, C. G. Formation and stability of G-quadruplexes self-assembled from guanine-rich strands. *Chem.—Eur. J.* **2007**, *13*, 945–949.

(32) Crnugelj, M.; Sket, P.; Plavec, J. Small change in a G-rich sequence, a dramatic change in topology: New dimeric G-quadruplex folding motif with unique loop orientations. *J. Am. Chem. Soc.* **2003**, *125*, 7866–7871.

(33) Dai, J. X.; Carver, M.; Punchihewa, C.; Jones, R. A.; Yang, D. Z. Structure of the Hybrid-2 type intramolecular human telomeric G-quadruplex in K^+ solution: insights into structure polymorphism of the human telomeric sequence. *Nucleic Acids Res.* **2007**, *35*, 4927–4940.

(34) Li, J.; Correia, J. J.; Wang, L.; Trent, J. O.; Chaires, J. B. Not so crystal clear: the structure of the human telomere G-quadruplex in solution differs from that present in a crystal. *Nucleic Acids Res.* **2005**, *33*, 4649–4659.

(35) Marathias, V. M.; Bolton, P. H. Determinants of DNA quadruplex structural type: Sequence and potassium binding. *Biochemistry* **1999**, *38*, 4355–4364.

(36) Phan, A. T.; Kuryavyi, V.; Luu, K. N.; Patel, D. J. Structure of two intramolecular G-quadruplexes formed by natural human telomere sequences in K^+ solution. *Nucleic Acids Res.* **2007**, *35*, 6517–6525.

(37) Phan, A. T.; Luu, K. N.; Patel, D. J. Different loop arrangements of intramolecular human telomeric (3 + 1) G-quadruplexes in K^+ solution. *Nucleic Acids Res.* **2006**, *34*, 5715–5719.

(38) Risitano, A.; Fox, K. R. Inosine substitutions demonstrate that intramolecular DNA quadruplexes adopt different conformations in the presence of sodium and potassium. *Bioorg. Med. Chem. Lett.* **2005**, *15*, 2047–2050.

(39) Vorlickova, M.; Chladkova, J.; Kejnovska, I.; Fialova, M.; Kypr, J. Guanine tetraplex topology of human telomere DNA is governed by the number of (TTAGGG) repeats. *Nucleic Acids Res.* **2005**, *33*, 5851–5860.

(40) Lilley, D. M. J. Structures of helical junctions in nucleic acids. *Q. Rev. Biophys.* **2000**, *33*, 109–159.

(41) Agrawal, S.; Ojha, R. P.; Maiti, S. Energetics of the human Tel-22 quadruplex-telomestatin interaction: A molecular dynamics study. *J. Phys. Chem. B* **2008**, *112*, 6828–6836.

(42) Arora, A.; Balasubramanian, C.; Kumar, N.; Agrawal, S.; Ojha, R. P.; Maiti, S. Binding of berberine to human telomeric quadruplex - spectroscopic, calorimetric and molecular modeling studies. *FEBS J.* **2008**, *275*, 3971–3983.

(43) Cavallari, M.; Calzolari, A.; Garbesi, A.; Di Felice, R. Stability and migration of metal ions in G4-wires by molecular dynamics simulations. *J. Phys. Chem. B* **2006**, *110*, 26337–26348.

(44) Clay, E. H.; Gould, I. R. A combined QM and MM investigation into guanine quadruplexes. *J. Mol. Graphics Modell.* **2005**, *24*, 138–146.

(45) Fadrna, E.; Spackova, N.; Stefl, R.; Koca, J.; Cheatham, T. E.; Sponer, J. Molecular dynamics simulations of guanine quadruplex loops: Advances and force field limitations. *Biophys. J.* **2004**, *87*, 227–242.

(46) Gu, J. D.; Leszczynski, J. Origin of Na^+/K^+ selectivity of the guanine tetraplexes in water: The theoretical rationale. *J. Phys. Chem. A* **2002**, *106*, 529–532.

(47) Han, H. Y.; Langley, D. R.; Rangan, A.; Hurley, L. H. Selective interactions of cationic porphyrins with G-quadruplex structures. *J. Am. Chem. Soc.* **2001**, *123*, 8902–8913.

(48) Hazel, P.; Huppert, J.; Balasubramanian, S.; Neidle, S. Loop-length-dependent folding of G-quadruplexes. *J. Am. Chem. Soc.* **2004**, *126*, 16405–16415.

(49) Hazel, P.; Parkinson, G. N.; Neidle, S. Predictive modelling of topology and loop variations in dimeric DNA quadruplex structures. *Nucleic Acids Res.* **2006**, *34*, 2117–2127.

(50) Chowdhury, S.; Bansal, M. A nanosecond molecular dynamics study of antiparallel $d(G)_7$ quadruplex structures: Effect of the coordinated cations. *J. Biomol. Struct. Dyn.* **2001**, *18*, 647–669.

(51) Chowdhury, S.; Bansal, M. G-quadruplex structure can be stable with only some coordination sites being occupied by cations: A six-nanosecond molecular dynamics study. *J. Phys. Chem. B* **2001**, *105*, 7572–7578.

(52) Meng, F. C.; Wang, F. P.; Zhao, X.; Jalbout, A. F. Guanine tetrad interacting with divalent metal ions ($M = Fe^{2+}$, Co^{2+}, Ni^{2+}, Cu^{2+} and Zn^{2+}): A density functional study. *J. Mol. Struct.-Theochem* **2008**, *854*, 26–30.

(53) Meyer, M.; Hocquet, A.; Suhnel, J. Interaction of sodium and potassium ions with sandwiched cytosine-, guanine-, thymine-, and uracil-base tetrads. *J. Comput. Chem.* **2005**, *26*, 352–364.

(54) Meyer, M.; Steinke, T.; Brandl, M.; Suhnel, J. Density functional study of guanine and uracil quartets and of guanine quartet/metal ion complexes. *J. Comput. Chem.* **2001**, *22*, 109–124.

(55) Meyer, M.; Suhnel, J. Density functional study of adenine tetrads with N6-H6. .N3 hydrogen bonds. *J. Phys. Chem. A* **2008**, *112*, 4336–4341.

(56) Ourliac-Garnier, I.; Elizondo-Riojas, M. A.; Redon, S.; Farrell, N. P.; Bombard, S. Cross-links of quadruplex structures from human telomeric DNA by dinuclear platinum complexes show the flexibility of both structures. *Biochemistry* **2005**, *44*, 10620–10634.

(57) Pagano, B.; Mattia, C. A.; Cavallo, L.; Uesugi, S.; Giancola, C.; Fraternali, F. Stability and cations coordination of DNA and RNA 14-mer G-quadruplexes: A multiscale computational approach. *J. Phys. Chem. B* **2008**, *112*, 12115–12123.

(58) Petraccone, L.; Erra, E.; Esposito, V.; Randazzo, A.; Mayol, L.; Nasti, L.; Barone, G.; Giancola, C. Stability and structure of telomeric DNA sequences forming quadruplexes containing four G-tetrads with different topological arrangements. *Biochemistry* **2004**, *43*, 4877–4884.

(59) Read, M. A.; Neidle, S. Structural characterization of a guanine-quadruplex ligand complex. *Biochemistry* **2000**, *39*, 13422–13432.

(60) Ross, W. S.; Hardin, C. C. Iin-induced stabilization of the G-DNA quadruplex - free-energy perturbation studies. *J. Am. Chem. Soc.* **1994**, *116*, 6070–6080.

(61) Rueda, M.; Luque, F. J.; Orozco, M. G-quadruplexes can maintain their structure in the gas phase. *J. Am. Chem. Soc.* **2006**, *128*, 3608–3619.

(62) Spackova, N.; Berger, I.; Sponer, J. Nanosecond molecular dynamics simulations of parallel and antiparallel guanine quadruplex DNA molecules. *J. Am. Chem. Soc.* **1999**, *121*, 5519–5534.

(63) Spackova, N.; Berger, I.; Sponer, J. Structural dynamics and cation interactions of DNA quadruplex molecules containing mixed guanine/cytosine quartets revealed by large-scale MD simulations. *J. Am. Chem. Soc.* **2001**, *123*, 3295–3307.

(64) Spackova, N.; Cubero, E.; Sponer, J.; Orozco, M. Theoretical study of the guanine-6-thioguanine substitution in duplexes, triplexes, and tetraplexes. *J. Am. Chem. Soc.* **2004**, *126*, 14642–14650.

(65) Sponer, J.; Spackova, N. Molecular dynamics simulations and their application to four-stranded DNA. *Methods* **2007**, *43*, 278–290.

(66) Stefl, R.; Spackova, N.; Berger, I.; Koca, J.; Sponer, J. Molecular dynamics of DNA quadruplex molecules containing inosine, 6-thioguanine and 6-thiopurine. *Biophys. J.* **2001**, *80*, 455–468.

(67) Strahan, G. D.; Keniry, M. A.; Shafer, R. H. NMR structure refinement and dynamics of the K^+-$[d(G_3T_4G_3)]_2$ quadruplex via particle mesh Ewald molecular dynamics simulations. *Biophys. J.* **1998**, *75*, 968–981.

(68) Li, H.; Cao, E. H.; Gisler, T. Force-induced unfolding of human telomeric G-quadruplex: A steered molecular dynamics simulation study. *Biochem. Biophys. Res. Commun.* **2009**, *379*, 70–75.

(69) Meyer, M.; Suhnel, J. Interaction of cyclic cytosine-, guanine-, thymine-, uracil- and mixed guanine-cytosine base tetrads with K^+, Na^+ and Li^+ ions - A density functional study. *J. Biomol. Struct. Dyn.* **2003**, *20*, 507–517.

(70) Stefl, R.; Cheatham, T. E.; Spackova, N.; Fadrna, E.; Berger, I.; Koca, J.; Sponer, J. Formation pathways of a guanine-quadruplex DNA revealed by molecular dynamics and thermodynamic analysis of the substates. *Biophys. J.* **2003**, *85*, 1787–1804.

(71) Krishnan-Ghosh, Y.; Liu, D. S.; Balasubramanian, S. Formation of an interlocked quadruplex dimer by d(GGGT). *J. Am. Chem. Soc.* **2004**, *126*, 11009–11016.

(72) Baker, E. S.; Bernstein, S. L.; Gabelica, V.; De Pauw, E.; Bowers, M. T. G-quadruplexes in telomeric repeats are conserved in a solvent-free environment. *Int. J. Mass Spectrom.* **2006**, *253*, 225–237.

(73) Cornell, W. D.; Cieplak, P.; Bayly, C. I.; Gould, I. R.; Merz, K. M.; Ferguson, D. M.; Spellmeyer, D. C.; Fox, T.; Caldwell, J. W.; Kollman, P. A. A 2nd generation force field for the simulation of proteins, nucleic acids, and organic molecules. *J. Am. Chem. Soc.* **1995**, *117*, 5179–5197.

(74) Wang, J. M.; Cieplak, P.; Kollman, P. A. How well does a restrained electrostatic potential (RESP) model perform in calculating conformational energies of organic and biological molecules. *J. Comput. Chem.* **2000**, *21*, 1049–1074.

(75) Cheatham, T. E.; Cieplak, P.; Kollman, P. A. A modified version of the Cornell et al. *J. Biomol. Struct. Dyn.* **1999**, *16*, 845–862.

(76) Simmerling, C.; Miller, J. L.; Kollman, P. A. Combined locally enhanced sampling and Particle Mesh Ewald as a strategy to locate the experimental structure of a nonhelical nucleic acid. *J. Am. Chem. Soc.* **1998**, *120*, 7149–7155.

(77) Elber, R.; Karplus, M. Enhanced sampling in molecular dynamics - use of the time-dependent Hartree approximation for a simulation of carbon-monoxide diffusion through myoglobin. *J. Am. Chem. Soc.* **1990**, *112*, 9161–9175.

(78) Horvath, M. P.; Schultz, S. C. DNA G-quartets in a 1.86 angstrom resolution structure of an Oxytricha nova telomeric protein-DNA complex. *J. Mol. Biol.* **2001**, *310*, 367–377.

(79) Perez, A.; Marchan, I.; Svozil, D.; Sponer, J.; Cheatham, T. E.; Laughton, C. A.; Orozco, M. Refinenement of the AMBER force field for nucleic acids: Improving the description of alpha/gamma conformers. *Biophys. J.* **2007**, *92*, 3817–3829.

(80) Ode, H.; Matsuo, Y.; Neya, S.; Hoshino, T. Force Field Parameters for Rotation Around chi Torsion Axis in Nucleic Acids. *J. Comput. Chem.* **2008**, *29*, 2531–2542.

(81) Foloppe, N.; MacKerell, A. D. All-atom empirical force field for nucleic acids: I. Parameter optimization based on small molecule and condensed phase macromolecular target data. *J. Comput. Chem.* **2000**, *21*, 86–104.

(82) MacKerell, A. D.; Banavali, N.; Foloppe, N. Development and current status of the CHARMM force field for nucleic acids. *Biopolymers* **2000**, *56*, 257–265.

(83) Perez, A.; Lankas, F.; Luque, F. J.; Orozco, M. Towards a molecular dynamics consensus view of B-DNA flexibility. *Nucleic Acids Res.* **2008**, *36*, 2379–2394.

(84) Kollman, P. A.; Massova, I.; Reyes, C.; Kuhn, B.; Huo, S. H.; Chong, L.; Lee, M.; Lee, T.; Duan, Y.; Wang, W.; Donini, O.; Cieplak, P.; Srinivasan, J.; Case, D. A.; Cheatham, T. E. Calculating structures and free energies of complex molecules: Combining molecular mechanics and continuum models. *Acc. Chem. Res.* **2000**, *33*, 889–897.

(85) Srinivasan, J.; Cheatham, T. E.; Cieplak, P.; Kollman, P. A.; Case, D. A. Continuum solvent studies of the stability of DNA, RNA, and phosphoramidate - DNA helices. *J. Am. Chem. Soc.* **1998**, *120*, 9401–9409.

(86) Auffinger, P.; Hashem, Y. Nucleic acid solvation: from outside to insight. *Curr. Opin. Struct. Biol.* **2007**, *17*, 325–333.

(87) McDowell, S. E.; Spackova, N.; Sponer, J.; Walter, N. G. Molecular dynamics simulations of RNA: An in silico single molecule approach. *Biopolymers* **2007**, *85*, 169–184.

(88) Schultze, P.; Smith, F. W.; Feigon, J. Refined solution structure of the dimeric quadruplex formed from the Oxytricha telomeric oligonucleotide d(GGGGTTTTGGGG). *Structure* **1994**, *2*, 221–233.

(89) Phan, A. T.; Patel, D. J. Two-repeat human telomeric d(TAGGGTTAGGGT) sequence forms interconverting parallel and antiparallel G-quadruplexes in solution: Distinct topologies, thermodynamic properties, and folding/unfolding kinetics. *J. Am. Chem. Soc.* **2003**, *125*, 15021–15027.

(90) Xu, Y.; Noguchi, Y.; Sugiyama, H. The new models of the human telomere d[AGGG(TTAGGG)$_3$] in K^+ solution. *Bioorg. Med. Chem.* **2006**, *14*, 5584–5591.

(91) Ambrus, A.; Chen, D.; Dai, J. X.; Bialis, T.; Jones, R. A.; Yang, D. Z. Human telomeric sequence forms a hybrid-type intramolecular G-quadruplex structure with mixed parallel/antiparallel strands in potassium solution. *Nucleic Acids Res.* **2006**, *34*, 2723–2735.

(92) Jorgensen, W. L.; Chandrasekhar, J.; Madura, J. D.; Impey, R. W.; Klein, M. L. Comparison of simple potential functions for simulating liquid water. *J. Chem. Phys.* **1983**, *79*, 926–935.

(93) Berendsen, H. J. C.; Grigera, J. R.; Straatsma, T. P. The missing term in effective pair potentials. *J. Phys. Chem.* **1987**, *91*, 6269–6271.

(94) Joung, I. S.; Cheatham, T. E. Determination of alkali and halide monovalent ion parameters for use in explicitly solvated biomolecular simulations. *J. Phys. Chem. B* **2008**, *112*, 9020–9041.

(95) Dang, L. X. Mechanism and thermodynamics of ion selectivity in aqueous solutions of 18-crown-6 ether - a molecular dynamics study. *J. Am. Chem. Soc.* **1995**, *117*, 6954–6960.

(96) Case, D. A.; Darden, T. A.; Cheatham, T. E., III; Simmerling, C. L.; Wang, J.; Duke, R. E.; Luo, R.; Merz, K. M.; Pearlman, D. A.; Crowley, M.; Walker, R. C.; Zhang, W.; Wang, B.; Hayik, S.; Roitberg, A.; Seabra, G.; Wong, K. F.; Paesani, F.; Wu, X.; Brozell, S.; Tsui, V.; Gohlke, H.; Yang, L.; Tan, C.; Mongan, J.; Hornak, V.; Cui, G.; Beroza, P.; Mathews, D. H.; Schafmeister, C.; Ross, W. S.; Kollman, P. A. *AMBER 9*; University of California: San Francisco, 2006.

(97) Case, D. A.; Darden, T. A.; Cheatham, T. E., III; Simmerling, C. L.; Wang, J.; Duke, R. E.; Luo, R.; Merz, K. M.; Wang, B.; Pearlman, D. A.; Crowley, M.; Brozell, S.; Tsui, V.; Gohlke, H.; Mongan, J.; Hornak, V.; Cui, G.; Beroza, P.; Schafmeister, C.; Caldwell, J. W.; Ross, W. S.; Kollman, P. A. *AMBER 8*; University of California: San Francisco, 2004.

(98) Case, D. A.; Pearlman, D. A.; Caldwell, J. W.; Cheatham, T. E., III; Ross, W. S.; Simmerling, C. L.; Darden, T. A.; Merz, K. M.; Stanton, R. V.; Cheng, A. L.; Vincent, J. J.; Crowley, M.; Ferguson, D. M.; Radmer, R. J.; Seibel, G. L.; Singh, U. C.; Weiner, P. K.; Kollman, P. A. *AMBER 5*; University of California: San Francisco, 1997.

(99) Case, D. A.; Pearlman, D. A.; Caldwell, J. W.; Cheatham, T. E., III; Ross, W. S.; Simmerling, C. L.; Darden, T. A.; Merz, K. M.; Stanton, R. V.; Cheng, A. L.; Vincent, J. J.; Crowley, M.; Tsui, V.; Radmer, R. J.; Duan, Y.; Pitera, J.; Massova, I.; Seibel, G. L.; Singh, U. C.; Weiner, P. K.; Kollman, P. A. *AMBER 6*; University of California: San Francisco, 1999.

(100) Case, D. A.; Pearlman, D. A.; Caldwell, J. W.; Cheatham, T. E., III; Wang, J.; Ross, W. S.; Simmerling, C. L.; Darden, T. A.; Merz, K. M.; Stanton, R. V.; Cheng, A. L.; Vincent, J. J.; Crowley, M.; Tsui, V.; Gohlke, H.; Radmer, R. J.; Duan, Y.; Pitera, J.; Massova, I.; Seibel, G. L.; Singh, U. C.; Weiner, P. K.; Kollman, P. A. *AMBER 7*; University of California: San Francisco, 2002.

(101) Darden, T.; York, D.; Pedersen, L. Particle mesh Ewald - an N.logN method for Ewald sums in large systems. *J. Chem. Phys.* **1993**, *98*, 10089–10092.

(102) Ryckaert, J. P.; Ciccotti, G.; Berendsen, H. J. C. Numerical integration of Cartesian equations of motion of a system with constraints - molecular dynamics of n-alkanes. *J. Comput. Phys.* **1977**, *23*, 327–341.

(103) Berendsen, H. J. C.; Postma, J. P. M.; Vangunsteren, W. F.; Dinola, A.; Haak, J. R. Molecular dynamics with coupling to an external bath. *J. Chem. Phys.* **1984**, *81*, 3684–3690.

(104) Humphrey, W.; Dalke, A.; Schulten, K. VMD: Visual molecular dynamics. *J. Mol. Graph.* **1996**, *14*, 33–38.

(105) Lu, X. J.; Olson, W. K. 3DNA: a software package for the analysis, rebuilding and visualization of three-dimensional nucleic acid structures. *Nucleic Acids Res.* **2003**, *31*, 5108–5121.

(106) Reblova, K.; Fadrna, E.; Sarzynska, J.; Kulinski, T.; Kulhanek, P.; Ennifar, E.; Koca, J.; Sponer, J. Conformations of flanking bases in HIV-1 RNA DIS kissing complexes studied by molecular dynamics. *Biophys. J.* **2007**, *93*, 3932–3949.

(107) Spackova, N.; Sponer, J. Molecular dynamics simulations of sarcin-ricin rRNA motif. *Nucleic Acids Res.* **2006**, *34*, 697–708.

(108) Sitkoff, D.; Sharp, K. A.; Honig, B. Accurate calculation of hydration free energies using macroscopic solvent models. *J. Phys. Chem.* **1994**, *98*, 1978–1988.

(109) Honig, B.; Nicholls, A. Classical electrostatics in biology and chemistry. *Science* **1995**, *268*, 1144–1149.

(110) Brooks, B. R.; Bruccoleri, R. E.; Olafson, B. D.; States, D. J.; Swaminathan, S.; Karplus, M. CHARMM - a program for macromolecular energy, minimization, and dynamics calculations. *J. Comput. Chem.* **1983**, *4*, 187–217.

(111) Langley, D. R. Molecular dynamic simulations of environment and sequence dependent DNA conformations: The development of the BMS nucleic acid force field and comparison with experimental results. *J. Biomol. Struct. Dyn.* **1998**, *16*, 487–509.

(112) Marathias, V. M.; Bolton, P. H. Structures of the potassium-saturated, 2: 1, and intermediate, 1: 1, forms of a quadruplex DNA. *Nucleic Acids Res.* **2000**, *28*, 1969–1977.

(113) Svozil, D.; Sponer, J. E.; Marchan, I.; Perez, A.; Cheatham, T. E.; Forti, F.; Luque, F. J.; Orozco, M.; Sponer, J. Geometrical and electronic structure variability of the sugar-phosphate backbone in nucleic acids. *J. Phys. Chem. B* **2008**, *112*, 8188–8197.

(114) Razga, F.; Zacharias, M.; Reblova, K.; Koca, J.; Sponer, J. RNA kink-turns as molecular elbows: Hydration, cation binding, and large-scale dynamics. *Structure* **2006**, *14*, 825–835.

(115) Wang, Y.; Patel, D. J. Solution structure of the human telomeric repeat $d[AG_3(T_2AG_3)_3]$ G-tetraplex. *Structure* **1993**, *1*, 263–282.

(116) Anisimov, V. M.; Lamoureux, G.; Vorobyov, I. V.; Huang, N.; Roux, B.; MacKerell, A. D. Determination of electrostatic parameters for a polarizable force field based on the classical Drude oscillator. *J. Chem. Theory Comput.* **2005**, *1*, 153–168.

(117) Halgren, T. A.; Damm, W. Polarizable force fields. *Curr. Opin. Struct. Biol.* **2001**, *11*, 236–242.

CT900200K